Pol. J. Environ. Stud. Vol. XX, No. X (XXXX), 1-9
DOI: *10.15244/pjoes/213563* ONLINE PUBLICATION DATE: 2025-12-10

Original Research

Optimized Synthesis of Lanthanum-Modified {201}-Faceted TiO_2 for Enhanced Fluoride Adsorption

Zhen Zhou[1], Yaqin Yu[2]*, Yuan Cheng[1], Ningran Hou[1], Wen Ma[1], Xiaojun Fang[1]

[1]State Key Laboratory of Technologies in Space Cryogenic Propellants, Beijing Special Engineering Design and Research Institute, Beijing 100028, China
[2]Center for Environmental Metrology, National Institute of Metrology, Beijing 100029, China

Received: 13 July 2025
Accepted: 23 October 2025

Abstract

The imperative for efficient co-removal of arsenic (As) and fluoride (F^-) motivated the strategic immobilization of lanthanum (La) species onto {201}-faceted TiO_2 – a material exhibiting exceptional affinity toward arsenic species. Among three synthesis routes evaluated (incipient wetness impregnation, one-step solvothermal, and two-step hydrothermal methods), the two-step hydrothermal approach demonstrated superior fluoride sequestration performance. Subsequent optimization of synthesis pH and calcination temperature (pH = 7.5, 300°C) further enhanced F^- removal efficacy. Nevertheless, the significant disparity in ionic radii between La^{3+} (1.032 Å) and Ti^{4+} (0.605 Å) inhibits direct substitution within O–Ti–O bonds, limiting the formation of stable O–La–O configurations and consequently constraining fluoride uptake capacity. This study provides a foundational framework for fabricating multifunctional bimetallic oxides incorporating high-index facets for complex water remediation scenarios.

Keywords: arsenic and fluoride co-removal, bimetal oxide, surface hydroxyl density, high-index facets, precipitation pH threshold

Introduction

Elevated levels of arsenic (As) and fluoride (F^-) in drinking water sources pose a persistent challenge across extensive groundwater-dependent regions of China, including Inner Mongolia, Xinjiang, Guizhou, Shaanxi, Shanxi, and Qinghai. Remote rural communities within these areas experience disproportionately severe impacts due to their geographical isolation, small-scale decentralized water supply systems, and limited access to advanced water treatment technologies.

Furthermore, the ongoing shift of heavy industry from urban to rural settings has intensified the risk of industrial heavy metal contamination in groundwater resources. Alok Mittal et al. [1] synthesized thorium oxide-modified multiwall carbon nanotubes and investigated their Pb(II) adsorption performance under varying temperatures and pH conditions. Moonis Ali Khan and coworkers [2] converted a byproduct

*e-mail: yuyq@nim.ac.cn
Tel.: +86-10-64524948
Fax: +86-10-64524948

of the oil industry (sesame oil cake) into hydrochar through hydrothermal treatment, exhibiting the highest Pb(II) adsorption capacity (24.57 mg/g) at 200°C, 6 h. Silicate mesoporous materials have garnered significant attention for heavy metal separation, such as Hg, Ag, and Cd ions, due to their high surface area and uniform pore structure, as reviewed by Zeid A. Alothman [3]. A novel silica-coated copper ferrite-decorated oxidized multi-walled carbon nanotube nanocomposite was synthesized by Saikh Mohammad Wabaidur et al. [4] via co-precipitation and hydrothermal methods, demonstrating efficient adsorption of cationic dyes (methylene blue and celestine blue) from aqueous solutions. El-Refaie Kenawy and coworkers [5] synthesized and characterized a CTAB-intercalated, branched polyhydroxystyrene-functionalized montmorillonite nanocomposite, which exhibited excellent sequestration capacity for cationic dyes (rhodamine B, crystal violet, and methylene blue) in aqueous environments.

Consequently, developing effective technologies for the simultaneous removal of As, F^-, and co-occurring heavy metals is of critical practical significance for safeguarding these vulnerable populations.

Adsorption represents a promising approach for heavy metal remediation in groundwater, offering a favorable balance between cost and performance. Titanium dioxide (TiO_2) has been widely employed as an adsorbent/filter medium, demonstrating strong affinity for metalloids like arsenic. However, its efficacy in fluoride removal remains suboptimal.

Previous work by our group synthesized TiO_2 crystals predominantly exposing high-index {201} facets [6-9]. In crystallography, high-index facets refer to a category of crystal facets characterized by their Miller indices {hkl}, where at least one of the three indices (h, k, or l) has an absolute value exceeding 1. As illustrated in Fig. 1, the {201} facet exhibits the largest Ti-O-Ti bond angle (150°) and Ti-O bond length (2.01 Å) compared to common low-index facets ({001}, {100}, {101}). This unique atomic configuration confers two key advantages: (1) The extended Ti-O distance reduces electron density around surface Ti atoms. According to Lewis acid-base theory, these electron-deficient Ti sites exhibit enhanced coordination affinity for As(III/V) species. (2) The intrinsically higher surface energy ({201} (1.72 J/m^2)>{001} (0.90 J/m^2)>{010} (0.53 J/m^2)>{101} (0.44 J/m^2)) and reactivity of the {201} facet contribute to superior arsenic adsorption capacity. Nonetheless, its performance for fluoride sequestration is inadequate.

Substantial research [10-14] indicated that incorporating rare earth elements (REEs) significantly enhanced the fluoride uptake capability of TiO_2-based adsorbents. For instance, Li et al. [12] synthesized TiO_2-La and TiO_2-Ce composites via hydrolytic co-precipitation, achieving maximum fluoride adsorption capacities of 15.1 mg/g and 9.6 mg/g, respectively. Jing et al. [13] engineered a composite adsorbent integrating TiO_2, LaOOH, and activated carbon for concurrent

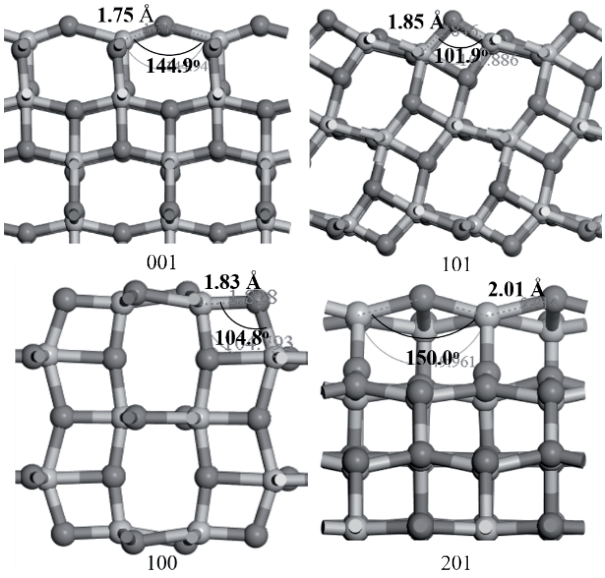

Fig. 1. Calculated bond lengths and bond angles for low-index ({001}, {100}, {101}) and high-index {201} TiO_2 facets. All the optimized geometries were performed utilizing density function theory (DFT) [5, 11-15].

As(III/V) and F^- removal, demonstrating high adsorption affinity for both contaminants. Yan et al. [14] epitaxially grafted lanthanum oxide nanostructures onto TiO_2 {100} facets via oriented growth, achieving efficient co-removal of As(III) and F^-. Lanthanum ions (La^{3+}), characterized by their high charge density and classification as hard Lewis acids, exhibit strong binding affinity with fluoride ions (hard Lewis bases). Additionally, lanthanum possesses a relatively low toxicity profile, with no significant adverse effects documented at low exposure levels. It is also not currently listed as a regulated contaminant in drinking water standards [15].

Motivated by these findings, we proposed the strategic immobilization of lanthanum species onto {201}-faceted TiO_2 to augment its fluoride removal performance while leveraging its inherent high arsenic adsorption capacity.

Materials and Methods

Materials

All chemical reagents were commercially procured and used without further purification. Sodium fluoride (NaF), lanthanum(III) nitrate hexahydrate ($La(NO_3)_3 \cdot 6H_2O$), glacial acetic acid (HAc), N,N-dimethylformamide (DMF), titanium(IV) butoxide (TBOT), nitric acid (HNO_3), and ammonium hydroxide ($NH_3 \cdot H_2O$) were acquired from Sinopharm Chemical Reagent Co., Ltd. (China) at analytical grade. A fluoride stock solution (1000 mg/L F^-) was prepared using ultrapure water (18.2 MΩ·cm, Milli-Q, USA). All solutions were stored at 4°C and used as required.

Synthesis of {201}-faceted TiO_2

{201}-faceted TiO_2 was synthesized via a modified solvothermal method [7]. Briefly, 8 mL glacial acetic acid (HAc) was introduced into a 50 mL Teflon-lined autoclave containing 12 mL N,N-dimethylformamide (DMF) under magnetic stirring. After thorough mixing, 0.5 mL titanium(IV) butoxide (TBOT) was added dropwise with continuous agitation. The sealed autoclave was transferred to a vacuum oven, heated from ambient temperature to 210ºC, and maintained at this temperature for 12 h, followed by passive cooling to room temperature. The resultant precipitate was collected by high-speed centrifugation (12,000 rpm), washed five times with absolute ethanol, and dried at 60ºC for 12 h. The dried product was ground into a fine powder prior to use.

Synthesis of Lanthanum-Modified {201} TiO_2

Impregnation Method

A 150 mg portion of {201}-faceted TiO_2 was dispersed in 20 mL aqueous $La(NO_3)_3 \cdot 6H_2O$ solution (0.25, 0.5, 1.0, and 1.5 M) under sonication for 8 h. The mixture was oven-dried at 60ºC, followed by calcination in a muffle furnace at 500ºC for 4 h (ramp rate: 5ºC/min). The resulting solid was ground, sieved, and washed thrice with ultrapure water. After final drying at 60ºC, the La-modified adsorbent was stored for characterization.

One-Step Solvothermal Method

La-incorporated {201} TiO_2 composites were synthesized via a modified single-step solvothermal route. Initially, 8 mL HAc was mixed with 12 mL DMF. Subsequently, 0.5 mL TBOT and varying masses of $La(NO_3)_3 \cdot 6H_2O$ (4.33 g, 0.866 g, 0.0866 g, or 0.00866 g) were added sequentially. After homogenization, the solution was transferred to a 100 mL Teflon-lined autoclave and reacted at 210ºC for 12 h. The precipitate was collected by centrifugation, rinsed with ethanol, dried at 60ºC, and sieved.

Two-Step Hydrothermal Method

Hydrothermal modification: 100 mg {201}-faceted TiO_2 was mixed with $La(NO_3)_3 \cdot 6H_2O$ (8.7, 866, 1732, or 4330 mg) in 20 mL ultrapure water to achieve La^{3+} concentrations of 1, 100, 200, or 500 mM. The suspension was hydrothermally treated at 210ºC for 12 h in a 50 mL autoclave.

Post-calcination: Solids were recovered, washed thrice with ultrapure water, dried, and calcined at 500ºC for 4 h (5ºC/min ramp).

Parameter optimization:

1) pH effect: $La(NO_3)_3$ solutions were adjusted to pH 2–12 using HNO_3/$NH_3 \cdot H_2O$ prior to adding TiO_2.
2) Calcination temperature: Composites prepared with 100 mg TiO_2 and 866 mg $La(NO_3)_3 \cdot 6H_2O$ (100 mM La^{3+}, pH 7.5) were calcined at 300, 400, or 500ºC.

Material Characterization

The surface morphology of La-modified {201} TiO_2 was characterized by field-emission scanning electron microscopy (FE-SEM, Hitachi S-3000N, Tokyo, Japan). Elemental composition analysis pre- and post-adsorption was performed using energy-dispersive X-ray spectroscopy (EDS) coupled to the same instrument. Crystal structure was determined via Raman spectroscopy (LabRAM HR Evolution, Horiba, Kyoto, Japan) with a 532 nm excitation laser. Fluoride ion (F^-) concentrations in aqueous solutions were quantified using an Orion fluoride ion-selective electrode (Thermo Fisher Scientific, Massachusetts, USA). Leached lanthanum ions were analyzed by inductively coupled plasma optical emission spectrometry (ICP-OES, PerkinElmer Optima 8000, Massachusetts, USA).

Batch Adsorption Experiments

A 5 mg/L fluoride (F^-) solution containing 0.04 M NaCl background electrolyte was prepared in a 500 mL beaker. Adsorbents ({201} TiO_2 or La-modified {201} TiO_2 were introduced at a solid-to-liquid ratio of 0.5 g/L. After homogenization, 40 mL aliquots were transferred into 50 mL Teflon-lined centrifuge tubes. The solution pH was adjusted to 7.0±0.1 using dilute HNO_3 or $NH_3 \cdot H_2O$. The tubes were agitated on an orbital shaker (200 rpm) at 25±1ºC. Periodic pH monitoring and adjustment were performed at 4-hour intervals to maintain stability (±0.2 pH units). Upon pH stabilization, solids were recovered via high-speed centrifugation (10,000×g, 10 min) and stored at 4ºC. The supernatant was filtered (0.22 μm nylon membrane), acidified with 2% (v/v) HNO_3, and analyzed for residual F^- concentration using an ion-selective electrode.

Results and Discussion

Impregnation Synthesis of La-Modified {201} TiO_2

The fluoride removal efficiency of La-impregnated {201} TiO_2 composites was evaluated in batch systems (5 mg/L F^-, pH 7.0). As depicted in Fig. 2, no notable enhancement in F^- removal was observed at any of the La impregnation concentrations (0.25-1.5 M). Conversely, adsorption capacity exhibited a slight decline with increasing La loading (e.g., 11.6% removal at 0.25 M vs. 10.3% at 1.5 M). This inverse trend suggested the ineffective immobilization of La species onto the {201} TiO_2 substrate.

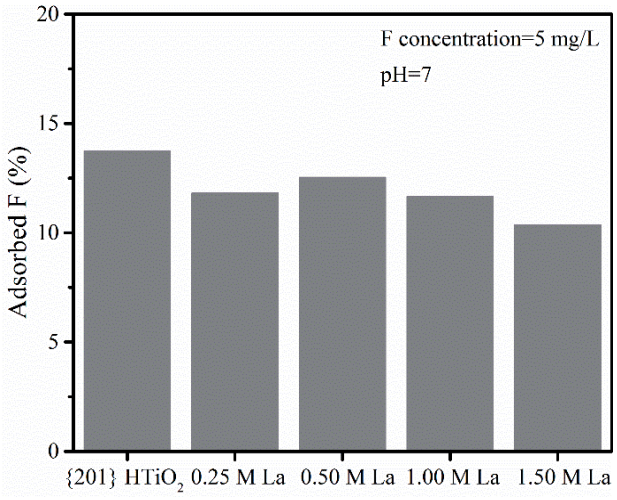

Fig. 2. Fluoride removal efficiency of {201}-faceted TiO_2 composites impregnated at varying La concentrations.

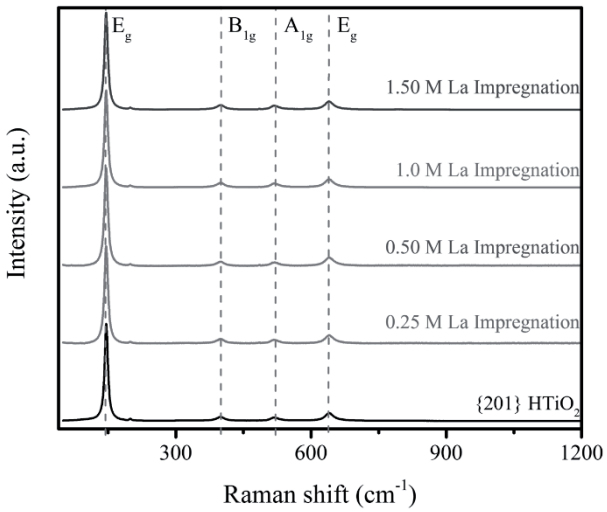

Fig. 4. Raman spectra of {201}-faceted TiO_2 impregnated with 0-1.5 M $La(NO_3)_3$ solutions via the impregnation method.

To verify La incorporation, EDS elemental mapping was performed (Fig. 3). Characteristic La Lα peaks (expected at 4.65 keV) were indistinguishable from overlapping Ti Kβ emissions (4.93 keV). Given the dominant Ti signal intensity and insufficient spectral resolution, definitive identification of La within the composite matrix was unattainable (cf. Fig. 3(a-d)).

Raman spectra (Fig. 4(a-e)) confirmed structural preservation of anatase TiO_2 after impregnation, evidenced by characteristic modes [16] at:

- 147 cm^{-1} (*E*g, symmetric O-Ti-O bending)
- 399 cm^{-1} (B_1g, O-Ti-O anti-symmetric bending)
- 518 cm^{-1} (A_1g, O-Ti-O symmetric stretching)
- 642 cm^{-1} (*E*g, Ti-O-Ti symmetric stretching)

Critically, no detectable peaks emerge in the 1050-1100 cm^{-1} region – the diagnostic spectral window for La_2O_3 (*e.g.*, the υ_1 symmetric La-O stretching mode at 1070 cm^{-1}) [14]. This absence confirms: 1) no crystalline La_2O_3 formation on {201} facets, and 2) the failure of La incorporation via impregnation,

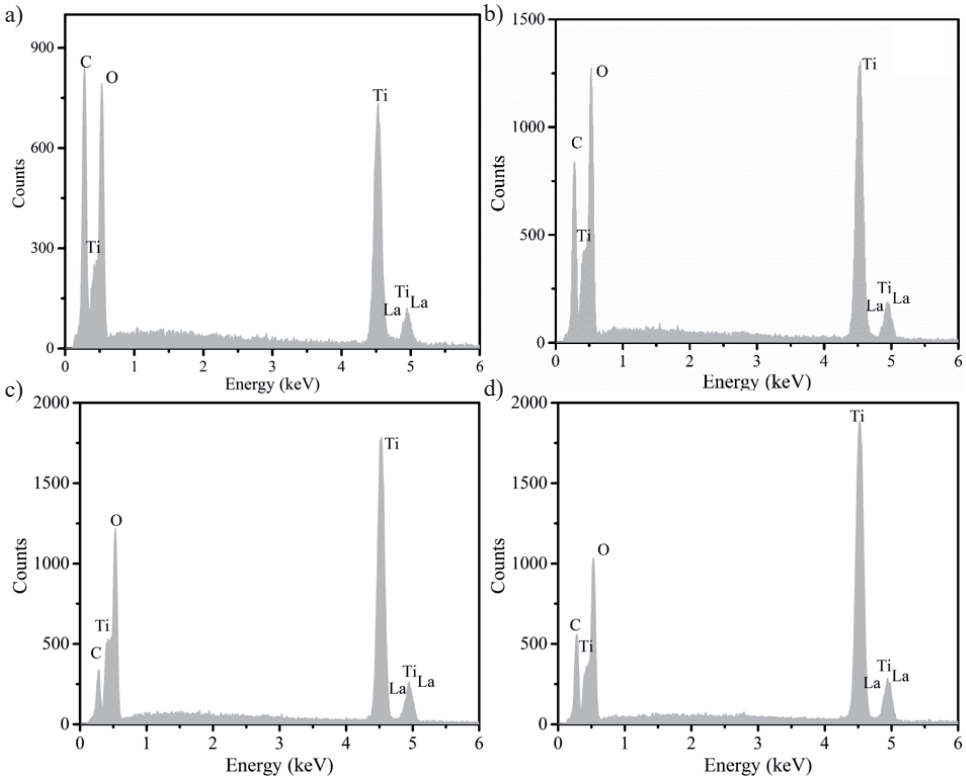

Fig. 3. EDS pattern of La impregnation {201} TiO_2 with a) 0.25, b) 0.5, c) 1.0, and d) 1.5 M La concentration.

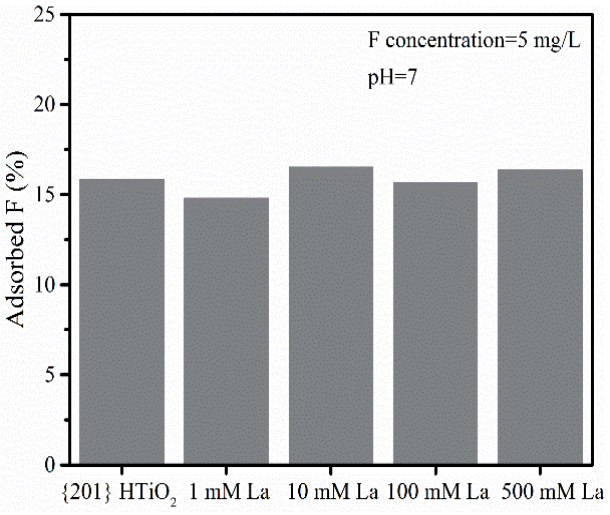

Fig. 5. Fluoride removal efficiency of La-modified {201} TiO_2 synthesized via one-step solvothermal method at varying La concentrations (1, 10, 100, 500 mM).

thereby rationalizing the negligible F^- adsorption enhancement (cf. Fig. 2).

One-Step Solvothermal Synthesis of La-Modified {201} TiO_2

The assessment of fluoride removal (5 mg/L F^-, pH 7.0) showed negligible enhancement (<17%) across the solvothermally synthesized La-TiO_2 composites, regardless of the La concentration (1-500 mM, Fig. 5). Motivated by the persistent inefficiency, we conducted a structural interrogation via FE-SEM (Fig. 6).

Morphological degradation was concentration-dependent: 1) at 1-10 mM La, diminished {201} facet expression (Fig. 6(a-b)), 2) at ≥100 mM, amorphous aggregates replacing the crystalline architecture (Fig. 6(c-d)).

Multi-modal characterization (Fig. 7) resolved the paradox: 1) EDS mapping (a-d): Spatially correlated Ti/La distribution (*Pearson's* $R \geq 0.79$), 2) point EDS (e): unresolved Ti Kβ (4.93 keV) and La Lα (4.65 keV) peaks, 3) Raman spectra (f): no emerging vibrational modes at 150-350 cm^{-1} (Ti-O-La bending) and 1000-1100 cm^{-1} (La-O stretching).

The spectroscopic absence of La-O-Ti bonds reduced the composite to a non-interacting physical mixture, inherently lacking coordination sites competent for fluoride chemisorption.

Two-Step Hydrothermal Synthesis of La-Modified {201} TiO_2

Fig. 8 depicts the fluoride (F^-) removal efficiency of the synthesized materials using a 5 mg/L F^- solution. The single-point adsorption data revealed that incorporating La into the {201} TiO_2 structure via the two-step hydrothermal method yielded a modest enhancement in F^- removal compared to pristine {201} TiO_2. Removal efficiency demonstrated a positive dependence on La precursor concentration. However, the incremental improvement in F^- removal diminished significantly within the La concentration range of 200-500 mM, and the overall removal performance remained unsatisfactory. Consequently, strategies beyond simply increasing La precursor concentration were explored to achieve higher F^- removal capacity.

Optimization of Synthesis pH

The synthesis pH was first investigated as a critical parameter. The initial La adsorption onto {201} TiO_2 was treated as a key preparatory step. Specifically,

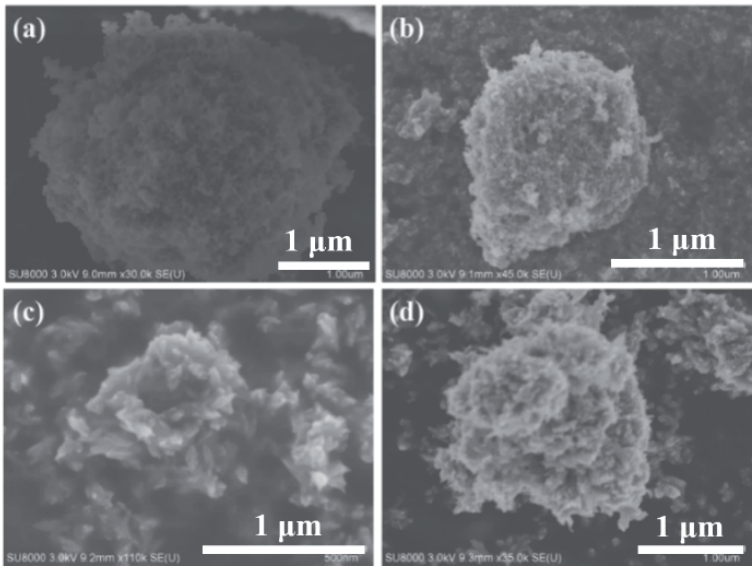

Fig. 6. FE-SEM of solvothermal products at La concentrations: a) 1 mM, b) 10 mM, c) 100 mM, d) 500 mM.

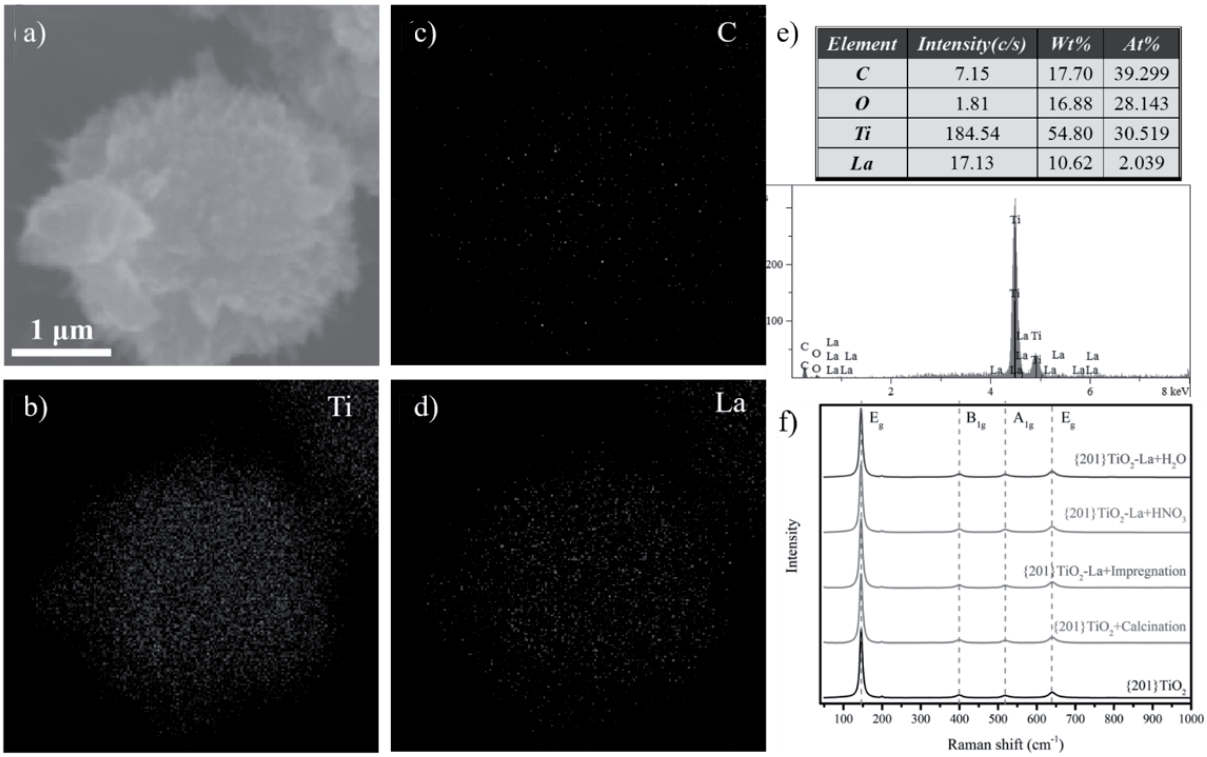

Element	Intensity(c/s)	Wt%	At%
C	7.15	17.70	39.299
O	1.81	16.88	28.143
Ti	184.54	54.80	30.519
La	17.13	10.62	2.039

Fig. 7. a-d) EDS elemental maps at 500 mM La; e) EDS spectrum showing Ti/La overlap; f) Raman spectra across La concentrations produced via the solvothermal method.

it is hypothesized that a higher La surface loading would promote more extensive oriented growth during the subsequent hydrothermal step, ultimately yielding a composite with enhanced F^- affinity and thus higher removal efficiency. Given the pronounced influence of solution pH on adsorption phenomena, pH edge experiments were conducted using {201} TiO_2 as the adsorbent and $La(NO_3)_3$ as the adsorbate. The solution pH was adjusted using HNO_3 and $NH_3{\cdot}H_2O$ to identify the optimal pH for maximizing La adsorption.

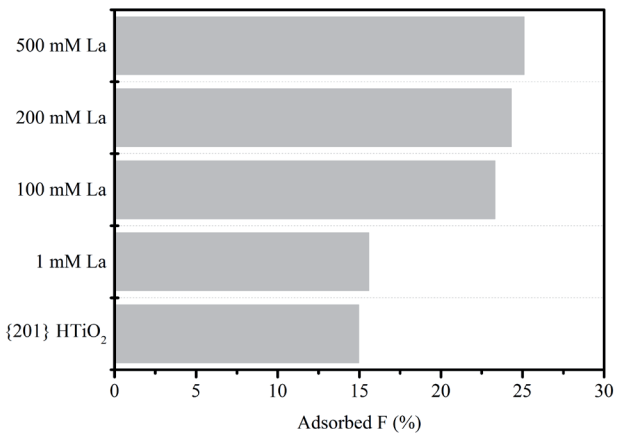

Fig. 8. Fluoride removal efficiency of {201} TiO_2-La composites synthesized at varying La concentrations (hydrothermal: 210°C, 12 h; calcination: 500°C, 4h).

Fig. 9 illustrates a marked increase in La adsorption onto {201} TiO_2 with rising pH. A sharp uptake surge occurred at pH>8, reaching near-complete adsorption at pH≥11. This behavior was attributed to the formation of $La(OH)_3$ surface precipitates under alkaline conditions (pH>8.67). The solubility product constant (Ksp) of $La(OH)_3$ at 25ºC is 1×10^{-19}, while the ion product of water (Kw) is 1×10^{-14}. According to dissolution equilibrium principles, precipitation occurs when the ion product (IP = $[La^{3+}][OH^-]^3$) exceeds Ksp. Therefore, for a 1 mM

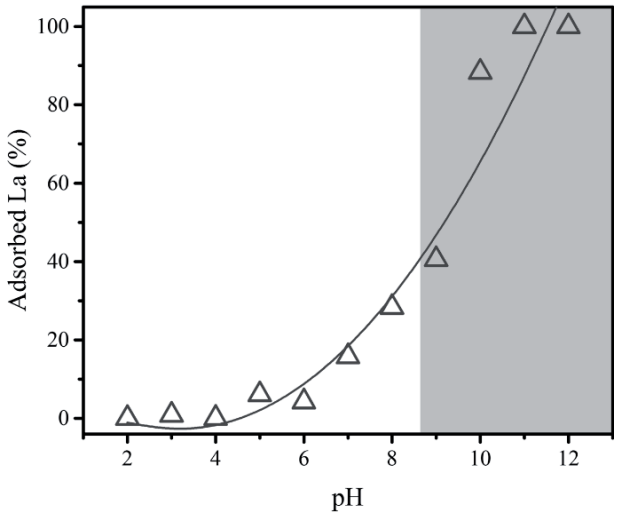

Fig. 9. Adsorption pH edge of La (1 mM) on 5 g/L {201} TiO_2.

La solution, the precipitation pH threshold (pH_{crit}) is calculated as follows:

$$IP = [La^{3+}][OH^-]^3 > Ksp \quad (1)$$

$$[H^+][OH^-] = K_W \quad (2)$$

$$pH = -\log[H^+] \quad (3)$$

Solving Equations (1), (2), and (3) yields:

$$\begin{aligned} pH_{crit} &= -\log[H^+] = -\log\left(\frac{K_w}{[OH^-]}\right) \\ &= \log\left[\left(\frac{K_{sp,La(OH)_3}}{[La^{3+}]}\right)^{\frac{1}{3}} \cdot \frac{1}{K_w}\right] \\ &= \frac{1}{3}\log\frac{K_{sp,La(OH)_3}}{[La^{3+}]} - \log K_w \\ &= 14 + \frac{1}{3}\log\frac{K_{sp,La(OH)_3}}{[La^{3+}]} \end{aligned} \quad (4)$$

Here, the pH_{crit} represents the precipitation pH threshold of $La(OH)_3$, the $K_{sp,\ La(OH)3}$ represents the solubility product constant of $La(OH)_3$, the $[H^+]$, $[OH^-]$, $[La^{3+}]$ respectively represent the H+, OH-, and La^{3+} ion concentrations in the solution.

The onset of $La(OH)_3$ formation in a 1 mM La solution is 8.67.

Therefore, the observed abrupt increase in adsorption is attributed to the onset of $La(OH)_3$ surface precipitation. Similarly, the precipitation onset pH for a 500 mM La solution is 7.77. Consequently, within the pH range below 7.77, La adsorption on {201} TiO_2 increased progressively with pH. The surface charge of TiO_2 was significantly affected by the pH value of the solution. The point of zero charge (PZC) of {201} TiO_2 is 6.5 [7]. When the pH values are lower than the PZC, the surface of {201} TiO_2 is positively charged because the surface hydroxyl groups (-OH) are protonated to form $-OH_2^+$; when the pH value is higher than the PZC, the surface is deprotonated to form $-O^-$, resulting in the surface negatively charged [7]. La(III) ions undergo hydrolysis in aqueous solutions, forming a series of hydroxyl complexes such as $La(OH)_2^+$, $La(OH)_2^+$, and $La(OH)_3$(aq) [17]. A positive correlation exists between the degree of hydrolysis and the pH value. At lower pH values, the main lanthanum species are free La^{3+} ions. With increasing pH, La^{3+} gradually hydrolyzes to form positively charged hydroxyl complexes. Thus, the hydrolysis products may be adsorbed onto the surface of {201} TiO_2 through electrostatic attraction, surface complexation, or ligand exchange. For practical synthesis control, the pH for subsequent synthesis steps was adjusted to 7.5.

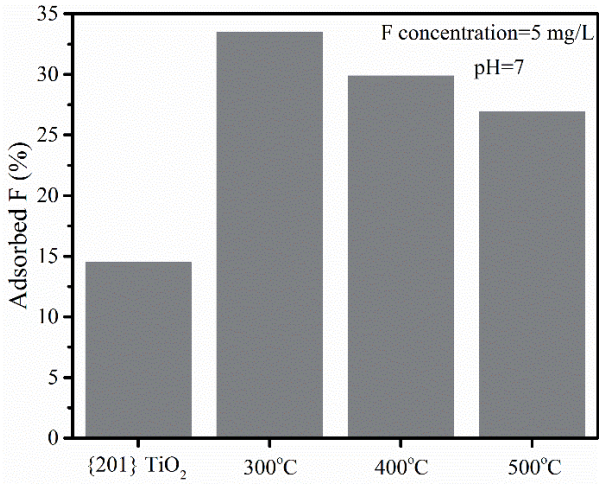

Fig. 10. Single-point adsorption of F (5 mg/L) on {201} TiO_2-La composites synthesized via the two-step method at different calcination temperatures.

Optimization of Calcination Temperature

Following La enrichment on the {201} TiO_2 surface, a calcination step is necessary to stabilize the La oxide phase. Given that the calcination temperature critically influences both the crystalline structure of the La oxide and the surface hydroxyl (OH) density – the latter being a key factor governing F^- adsorption capacity [18, 19] – we evaluated the effect of calcination temperature (300, 400, and 500ºC) on the F^- removal performance of the two-step hydrothermally synthesized adsorbent.

As shown in Fig. 10, calcination temperature exerts a significant influence on the material's F^- removal capability. Performance decreased progressively with increasing calcination temperature, showing an inverse relationship between calcination temperature and F^- removal efficiency. This decline was ascribed to alterations in surface OH density. Consistent with thermogravimetric analysis for {201} TiO_2, higher calcination temperatures facilitate the dehydration and removal of surface OH groups. Since surface OH groups constitute primary adsorption sites for F^-, their reduction directly diminishes F^- adsorption efficiency.

Conclusions

This study explored various composite synthesis strategies (impregnation, one-step solvothermal, and two-step hydrothermal methods) to incorporate La into {201} TiO_2 for fluoride removal. The two-step hydrothermal approach demonstrated superior F^- removal performance. Optimization of synthesis pH and calcination temperature yielded a maximum F^- removal efficiency of 33.5%. However, this efficiency level remains insufficient for practical compliance requirements. The limitations may stem from several factors:

1) Crystallographic Mismatch: The significant disparity in atomic radii (La^{3+}: ~1.061 Å vs. Ti^{4+}: ~0.605 Å) hinders stable substitutional doping within the TiO_2 lattice [20-22]. Attempted substitution likely induces severe crystallographic strain, preventing the formation of a stable doped structure.

2) Surface Energy Barrier: The high surface energy inherent to {201} TiO_2 facets (1.72 J/m^2> dopant integration threshold 1.25 J/m^2) [23, 24] creates a significant energy barrier that hinders effective doping via conventional methods.

3) Coordination Environment Incompatibility: The specific coordination requirements of La^{3+} may not be adequately met by the {201} TiO_2 surface environment, leading to surface reactions with active sites rather than successful lattice incorporation [25, 26].

Future research should consider alternative fluoride-affinitive elements, such as other rare earth elements (e.g., Cerium) or elements from the same group as Titanium (e.g., Zirconium). Alternatively, novel synthesis strategies could be pursued, including precise control over synthesis conditions, utilization of specialized doping precursors, or employing advanced techniques like Atomic Layer Deposition (ALD) to enhance the loading efficiency on high-index {201} TiO_2 facets, ultimately aiming for effective co-removal of arsenic and fluoride via bimetallic oxides.

Acknowledgments

This work was supported by the National Natural Science Foundation of China (Grant No. 42207259), Liaoning Province Science and Technology Project (Grant No. 2023-MSLH-099), National Institute of Metrology, China (Grant Nos. AKYJJ2307, 28-ZH2503, and AKYZZ2553).

Conflict of Interest

The authors declare no conflict of interest.

References

1. ALOK M., MU N., GAURAV S., ALOTHMAN Z.A., WABAIDUR S.M., MANAWWER A. Fabrication of MWCNTs/ThO_2 nanocomposite and its adsorption behavior for the removal of Pb(II) metal from aqueous medium. Desalination and Water Treatment. **57** (46), 21863, **2016**.
2. MOONIS A.K., AYOUB A.A., SAIKH M.W., MASOOM RAZA S., BYONG-HUN J., SHAREEFA A.A., ZEID A.A., ABDELRAZIG E.H. Oil industry waste based non-magnetic and magnetic hydrochar to sequester potentially toxic post-transition metal ions from water. Journal of Hazardous Materials. **400** (5), 123247, **2020**.
3. ALOTHMAN Z.A. A review: Fundamental aspects of silicate mesoporous materials. Materials. **5** (12), 2874, **2012**.
4. SAIKH M.W., MOONIS A.K., MASOOM R.S., MARTA O., BYONG-HUN J., ZEID A.A., AFNAN A.H.H. Oxygenated functionalities enriched MWCNTs decorated with silica coated spinel ferrite-A nanocomposite for potentially rapid and efficient de-colorization of aquatic environment. Journal of Molecular Liquids. **317** (1), 113916, **2020**.
5. EL-REFAIE K., AYMAN A.G., SAIKH M.W., MOONIS A.K., MASOOM R.S., ZEID A.A., AYOUB A.A., MUHAMMAD H. Cetyltrimethylammonium bromide intercalated and branched polyhydroxystyrene functionalized montmorillonite clay to sequester cationic dyes. Journal of Environmental Management. **219** (1), 285, **2018**.
6. ZHOU Z., YU Y., DING Z., ZUO M.M., CHENG J.M., JING C.Y. Competitive adsorption of arsenic and fluoride on {201} TiO_2. Applied Surface Science. **466**, 425, **2019**.
7. YU Y., ZHOU Z., DING Z., ZUO M.M., CHENG J.M., JING C.Y. Simultaneous arsenic and fluoride removal using {201} TiO_2-ZrO_2: Fabrication, characterization, and mechanism. Journal of Hazardous Materials. **377**, 267, **2019**.
8. ZHOU Z., YU Y., FANG X. Comparative study on the effects of {201} TiO_2 and {201} TiO_2−ZrO_2 on arsenite photocatalysis. Inorganic Chemistry Communications. **154**, 110945, **2023**.
9. YU Y., ZHOU Z., SONG X. Molecular-level insights into surface complexation of arsenite, selenium and cadmium on {201} TiO_2. Separation and Purification Technology. **332**, 125566, **2024**.
10. ZHOU Z., YU Y., DING Z. Modulating high-index facets on anatase TiO_2. European Journal of Inorganic Chemistry. **56**, 683, **2018**.
11. YAN X., SONG K., WANG J. Preparation of CeO_2-TiO_2/SiO_2 and its removal properties for fluoride ion. Journal of Rare Earths. **16** (4), 275, **1998**.
12. LI Z., DENG S., ZHANG X. Removal of fluoride from water using titanium-based adsorbents. Frontiers of Environmental Science and Engineering in China. **4** (4), 414, **2010**.
13. JING C., CUI J., HUANG Y. Fabrication, characterization, and application of a composite adsorbent for simultaneous removal of arsenic and fluoride. ACS Applied Materials & Interfaces. **4** (2), 714, **2012**.
14. YAN L., TU H., CHAN T. Mechanistic study of simultaneous arsenic and fluoride removal using granular TiO_2-La adsorbent. Chemical Engineering Journal. **313** (3), 983, **2017**.
15. TROFIMOVICH E.M. Hygiene standards of chemical elements of drinking water. Hygiene and Sanitation. **102** (2), 126, **2023**.
16. CASTREJÓN-SÁNCHEZ V.H., LÓPEZ R., RAMÓN-GONZÁLEZ M., ENRÍQUEZ-PÉREZ Á., CAMACHO-LÓPEZ M., VILLA-SÁNCHEZ G. Annealing control on the anatase/rutile ratio of nanostructured titanium dioxide obtained by sol-gel. Crystals. **9** (1), 22, **2018**.
17. RIDLEY M.K., MACHESKY M.L., KUBICKI J.D. Ion and particle size effects on the surface reactivity of anatase nanoparticle–aqueous electrolyte interfaces: Experimental, density functional theory, and surface complexation modeling studies. Minerals. **12** (7), 907, **2022**.
18. RAZA W., HAQUE M., MUNEER M. Photocatalytic degradation of different chromophoric dyes in aqueous phase using La and Mo doped TiO_2 hybrid carbon spheres. Journal of Alloys and Compounds. **632**, 837, **2015**.

19. SHI Q., YAN L., CHAN T. Arsenic adsorption on lanthanum-impregnated activated alumina: Spectroscopic and DFT study. ACS Applied Materials & Interfaces. **7** (48), 26735, **2015**.
20. LI G., CHEN K., JIN J. Synthesis and electrochemical properties of La^{3+}-doped NiCo layered double hydroxide nanosheets. Chinese Journal of Applied Chemistry. **34** (1), 71, **2017**.
21. BAI J., YANG J., LYU Z. Magnetic and dielectric properties of Ti^{4+}-doped M-type hexaferrite $BaFe_{12-x}Ti_xO_{19}$ ceramics. Journal of Inorganic Materials. **36** (1), 43, **2021**.
22. GATEA HAMED A., OBAID MAITHM A., MOHAMMED ABDULKAREEM M. Ionic radius effect on structural and electrical properties of barium strontium titanate thin films. Digest Journal of Nanomaterials and Biostructures. **19** (3), 1117, **2024**.
23. YAN J. Grain boundary segregation and barrier structure of TiO_2 varistor ceramics. Kunming University of Science and Technology, **2009**.
24. ANILKUMAR P., KALAIVANI T., DEEPAK S. Evaluation of structural, optical and morphological properties of La doped TiO_2 nanoparticles. Ceramics International. **49** (11), 16991, **2023**.
25. WANG R., AN S., ZHANG J. Existence form of lathanum and its improving mechanism of visible-light-driven La-F co-doped TiO_2. Journal of Rare Earths. **38** (1), 39, **2020**.
26. LI L., CHEN H., LI L. La-doped TiO_2 nanorods toward boosted electrocatalytic N_2-to-NH_3 conversion at ambient conditions. Chinese Journal of Catalysis. **42** (10), 1755, **2021**.